Reprinted from

Applied Physics Letters

Volume 51 19 October 1987 Number 16

Subboundary-free zone-melt recrystallization of thin-film silicon

Loren Pfeiffer, A. E. Gelman,[a] K. A. Jackson, K. W. West, and J. L. Batstone
AT&T Bell Laboratories, Murray Hill, New Jersey 07974

(Received 23 April 1987; accepted for publication 19 August 1987)

pp. 1256-1258

a publication of the American Institute of Physics

Subboundary-free zone-melt recrystallization of thin-film silicon

Loren Pfeiffer, A. E. Gelman,[a] K. A. Jackson, K. W. West, and J. L. Batstone
AT&T Bell Laboratories, Murray Hill, New Jersey 07974

(Received 23 April 1987; accepted for publication 19 August 1987)

Scanned zone-melt recrystallization (ZMR) of amorphous Si 1-μm films on SiO_2 results in subboundary-free material provided the thermal gradient along the scan is reduced to 4 K/mm or less. Below this value the usual ZMR subboundaries consisting of networks of in-plane edge dislocations are replaced by rows of threading dislocations. We account for the two kinds of crystallization by extending the faceted solidification model that we developed previously. We consider profiles of the solidification front at the intersections of {111} facet pairs where subboundaries are known to form, and postulate that the profiles are aligned approximately normal to the scan in the high gradient case, but become tilted toward the plane of the SiO_2 cap layer for the low gradient case. The tilting accounts in a natural way for subboundary removal and the transition from in-plane to threading dislocations.

Networks of low angle grain boundaries or subboundaries are the singular characteristic crystallographic defect[1,2] found in thin-film silicon zone-melt recrystallized (ZMR) on vitreous SiO_2 substrates. Essentially all of the recent work in ZMR of silicon-on-insulator (SOI) is aimed at eliminating subboundaries or in mitigating their effects. Recently in our laboratory and elsewhere large areas of subboundary-free thin-film ZMR SOI have been obtained.[3–7] In this letter we (i) show that subboundary-free ZMR Si is associated with a new kind of low-thermal-gradient solidification that is qualitatively distinct from the conventional thin-film recrystallization reported over the past decade or more and (ii) propose a physical model that ascribes the differences in the two recrystallization regimes to differences in the geometry of the liquid-freezing interface during growth.

The sharp transition between the two modes of SOI crystallization is shown in Fig. 1. The SOI structure for these experiments was made by the following recipe. Silicon (100) wafers of 100 mm diameter were steam oxidized to 2 μm, then 1 μm of amorphous Si was chemically vapor deposited (CVD) at 580 °C, followed by a 2×10^{15} cm^{-2} carbon implant at 100 keV (to improve ZMR wetting[8]), and completed with a 2.5-μm CVD SiO_2 cap layer at 450 °C. The wafer then was uniformly heated from the underside to 1470 K and melt scanned at 0.3 mm/s from left to right with a 4-mm-wide upper wire having a wafer-to-wire clearance of 2 mm. The temperature of the upper wire was adjusted near 2300 K to produce a melt zone only 0.8 mm wide during the portion of scan on the left side of Fig. 1. However, when the ZMR scan reached the middle of the micrograph, the power to the upper wire was abruptly increased by 12%. This increased the width of the molten zone to about 1.8 mm and resulted in the dramatic decline in film quality seen in the figure. The upper insets to the figure are electron channeling pattern (ECP) angular diffraction[9] measures of the crystallographic quality obtained using an electron beam with an ECP crossover located above the sample to increase the selected area on the sample. The film on the left is grain- and subboundary-free (100) silicon (that is, there are no subboundaries as large as 0.1°), but the material on the right after the power increase contains subgrains tilted at random angles within an angular radius of about 1.5° of the (100) axis.

Narrow-melt material differs in a qualitative way from wide-melt material. Subboundaries in the wide-melt material (top plan-view micrograph of Fig. 2) typically consist of vertical walls of edge dislocations (Burgers vector $\mathbf{b} = a/2$ [101]), which run in the plane of the film parallel to the [010] scan direction often for hundreds of microns.[2] Dislocations in the narrow-melt material are far less extended. Figure 2, bottom, shows no subboundaries, but typically rows of short screw dislocations ($\mathbf{b} = a/2$ [011]) that thread reasonably directly through the thickness of the silicon film terminating on the two encapsulating oxide layers. In other regions, these threading dislocations are clustered

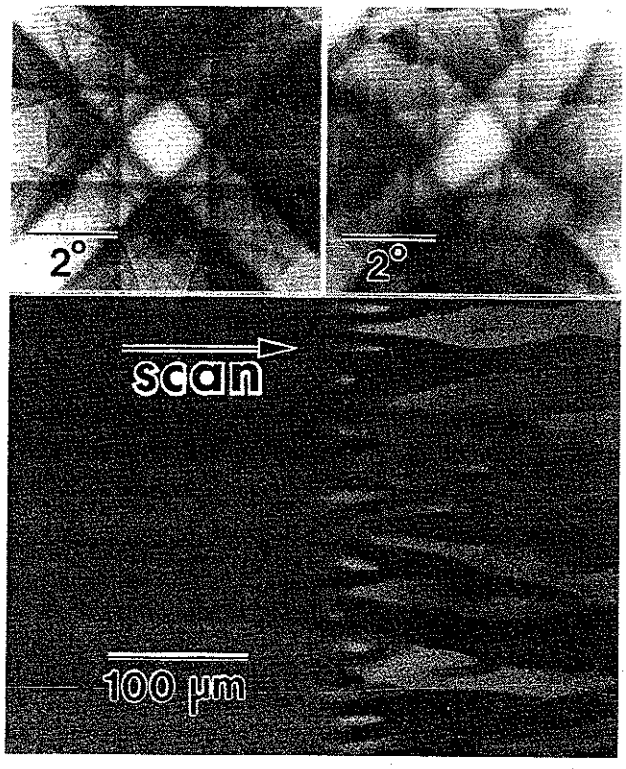

FIG. 1. Scanning electron micrograph in electron backscatter channeling contrast showing the abrupt change in SOI material quality as the ZMR scan is changed from the low-gradient condition (left), to the high-gradient condition (right). The insets are electron channeling pattern angular diffraction spectra of the two kinds of material.

[a] Present address: Dept. of Statistics, Harvard University, Cambridge, MA 02138.

 0003-6951/87/421256-03$01.00

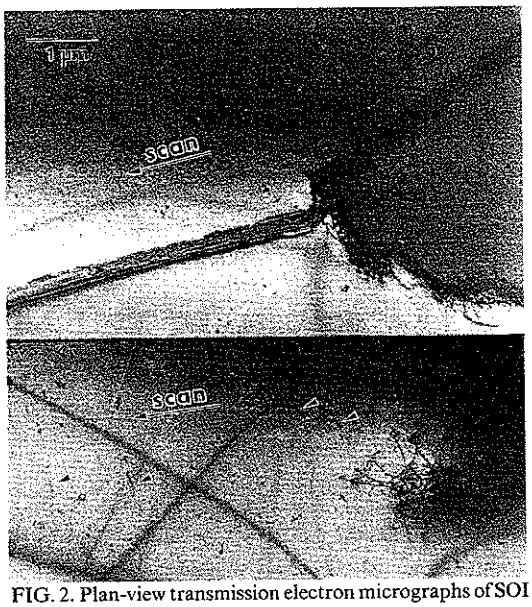

FIG. 2. Plan-view transmission electron micrographs of SOI subboundaries in the material of Fig. 1 imaged using a bright field (220) reflection. Top photo is a high-gradient subboundary showing a vertical array of edge dislocation running parallel to the scan direction in the plane of the Si film. Sample was titled towards ⟨112⟩ to reveal the individual dislocations in the wall. Bottom photo is a low-gradient subboundary showing rows of isolated threading dislocations at the left (marked with arrow tips) and a dislocation cluster at the right.

in rows of widely ($\sim 10\ \mu$m) separated knots.[4] One such cluster is shown at the right in the lower micrograph of Fig. 2.

An iterative finite element heat flow analysis of our ZMR experiment using a single upper heater wire in a close wire-to-wafer geometry, shows[10,11] that narrow-melt widths are associated with low thermal gradients in the Si film at the solidification front. We calculate that the narrow-melt-zone material at the left of Fig. 1 corresponds to a gradient along the scan of 3 K/mm, as compared to 15 K/mm for the material at the right.

Using this heat flow analysis as a guide we have constructed a model for these effects. Our starting point is the {111} faceted interface model developed by the MIT-Lincoln group[12] and ourselves[13] to account for the characteristic branched patterns formed by high-gradient ZMR subboundaries in silicon thin films. The models main features are as follows.

Strip heater ZMR Si films on SiO_2 are experimentally found to be (100) textured, and because ⟨010⟩ Si is a fast growth direction,[14] this tends to become the growth axis aligned in the direction of scan. Because ⟨111⟩ is the slowest Si growth direction,[14] the interface between the melt and the Si crystal is assumed to be everywhere terminated on the Si {111} crystal planes, and the growth on these planes is assumed to be nucleation limited. The subboundaries formed during ZMR are by experiment found in the solid at the interior corners formed by adjacent pairs of {111} interfacial facets. These assumptions with the analysis of Ref. 13 make it possible to generate the time development of the facets, and thus plot the loci of the interior corners, during faceted growth. The success of that model is the close correspondence that was found between these interior corner loci and the patterns formed by experimental subboundaries in ZMR silicon thin films.[13]

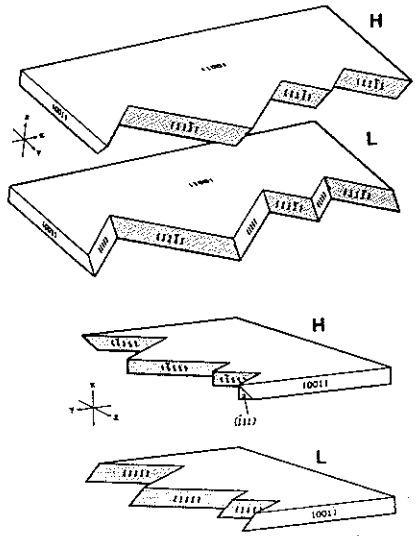

FIG. 3. Examples of possible {111} faceted growth interfaces. The high-thermal-gradient ZMR condition preferentially selects facet structures of the type labeled *H*, and the low-gradient condition selects type *L* structures.

Consider now this faceted melt-crystallization interface in three dimensions. It establishes itself on some set of Si {111} planes lying between the isothermal surfaces determined by the Si melting point and the temperature of maximum undercooling of the melt appropriate to the scan velocity. For (100) textured growth in the ⟨010⟩ direction any combination of the planes (111), (11$\bar{1}$), ($\bar{1}$11), or ($1\bar{1}$1) is a possible facet for the growth front. Two examples are illustrated in Fig. 3. The lower example in each view consists of only (111) and (11$\bar{1}$) facets; it is a simple upward-tilting snowplow shape with the lower silicon film surface crystallizing always ahead of that nearer the cap surface. Consider now the (111), (11$\bar{1}$) facet intersections. Profiles at both the exterior and interior corners as viewed from the solid extend forward at the bottom of the silicon film as compared to the top. On the other hand, for the upper example in Fig. 3, the ($\bar{1}$11) facet tilts downward, and the (11$\bar{1}$) facet upward. So for this case the facet intersections at both exterior and interior corners have vertical profiles as viewed down the length of the upper heater wire.

The actual faceted interface could consist of pure examples as illustrated or complex mixtures of these cases and their mirror reflections containing also ($1\bar{1}$1) facets. To get some guidance on how the faceted structure might be chosen in a given experiment, let us turn to another result obtained from the finite element thermal analysis.

Figure 4 shows the 1685 K silicon melting isotherm calculated from this analysis in the various SOI layers for both the high- and low-gradient cases of Fig. 1. Observe that the isotherm is nearly vertical in the 1-μm silicon film with the high gradient, but for the low gradient it is slanted toward the plane of the cap oxide indicating that the silicon film is $\sim$0.005 K hotter at its top than at its bottom surface. This suggests that high-gradient melt conditions should favor a facet geometry of the type ($\bar{1}$11), (11$\bar{1}$) because the vertical intersection profile most closely matches the near vertical high-gradient isotherm. Similarly, the low-gradient condition would be expected to favor facet pairs of the type (111), ($1\bar{1}$1), because both the isotherm and the profiles at the facet

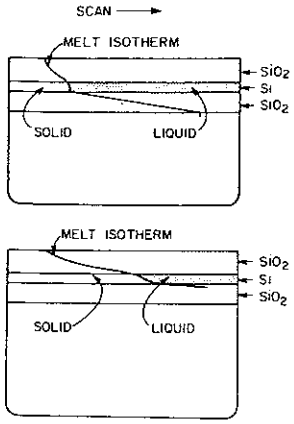

FIG. 4. Isotherm profiles in a 1-μm Si film for both high- and low-gradient conditions, calculated using the finite element differential heat flow analysis. The high-gradient case is at the top; the low-gradient case is at the bottom of the figure.

intersections are biased so that the bottom of the film crystallizes slightly ahead of the top.

We concentrated on the interior corner profiles formed by the intersections of adjacent {111} facets, because it is well established[1,4] that subboundary formation occurs there. These profiles are schematically summarized in Fig. 5 for ZMR growth moving towards the right at three instants. The liquid Si melt is symbolized by shading.

Consider now dislocation formation resulting from differential thermal stresses or impurity and particulate incorporation, and suppose these stresses can be relieved by a given formation rate for dislocations as the ZMR scan proceeds. These dislocations can propagate in the growing solid *only* by extending into the new material formed at the melt-solid interface. Studies in the literature show that dislocation propagation in a growing crystal tends to be favored in directions running approximately normal to the melt-solid interface.[15] Thus for the vertical recrystallization profile of high-gradient material, each new dislocation can propagate indefinitely in the horizontal plane of the Si film. As new dislocations are continually added to those already present, sizable cumulative crystallographic distortions build up as the subboundary is extended along the scan. However, for the slanted profile of the low-gradient material at the left in Fig. 5, the same rule of dislocation propagation normal to the melt-solid interface results in short threading dislocations which start at the bottom of the Si film and self-terminate at the cap oxide. This accounts both for the observed transition to threading dislocations, and because cumulative effects are prevented, for the markedly better crystallographic texture found in the low-gradient films.

Several other experimental observations are also explainable in the context of the model. Thus (i) the abruptness of the transition in Fig. 1 is understood because only a simple flipping of the {111} facet faces from the low to high gradient configuration is involved. (ii) The comparative ease in achieving low-gradient recrystallization with SOI films 1 μm thick and thicker is understood by the larger top to bottom temperature bias available for the thicker films. (iii) The high thermal gradients associated with focused lasers and electron beams account for the inability to achieve subboundary-free SOI by ZMR with these heat sources thus far, and suggest that by proper defocusing this might change. (iv) The alternating upward and downward facing facet configuration of the high-gradient case accounts for why the high-gradient subgrains have both β and γ tilt, as is demonstrated in Ref. 7, and why after flipping to the upward facing snowplow, the γ tilt is suddenly removed as the thermal gradient is reduced. (v) Finally, it is now clear why subboundary-free ZMR was in the past associated only with low scan velocities. For a strip heater with a single narrow upper heater wire, low-gradient conditions are obtained only with narrow melten zones and this results in peak temperatures only slightly above the Si melting point. For low scan velocities there is no problem with complete melting, but for higher velocity scans there is insufficient time to completely melt all of the polycrystalline Si feedstock, so high-velocity low-gradient scans result in large grain polycrystals. By increasing the width of the scanning upper heater to 4 mm, we are now able to routinely produce subboundary-free SOI films over entire 100-mm wafers using scan velocities in excess of 0.3 mm/s.

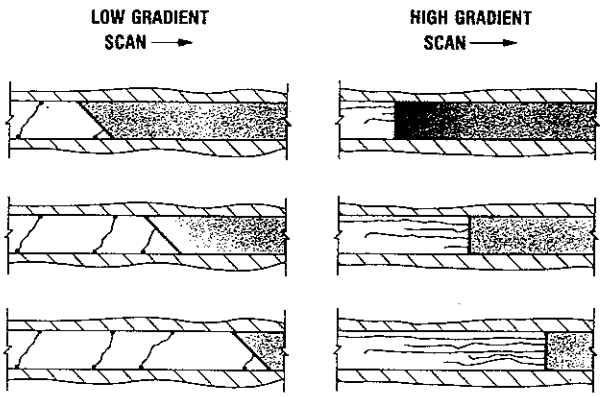

FIG. 5. Cross sections showing the postulated melt-solid profiles at the interior corners formed by the proposed facet configurations for the low- and high-gradient ZMR conditions. The figure also illustrates the proposed mechanism whereby high-gradient in-plane dislocations are transformed to threading dislocations as the thermal gradient is reduced below 4 K/mm.

[1]M. W. Geis, H. I. Smith, B-Y. Tsaur, J. C. C. Fan, D. J. Silversmith, and R. W. Mountain, J. Electrochem. Soc. **129**, 2812 (1982).
[2]M. Haond, D. P. Vu, and D. Bensahel, J. Appl. Phys. **54**, 3892 (1983), and also H. Baumgart and F. Phillip, Mater. Res. Soc. Symp. Proc. **35**, 593 (1985).
[3]Loren Pfeiffer, K. W. West, Scott Paine, and D. C. Joy, Mater. Res. Soc. Symp. Proc. **35**, 583 (1985).
[4]M. W. Geis, C. K. Chen, H. I. Smith, R. W. Mountain, and L. C. Doherty, Mater. Res. Soc. Symp. Proc. **35**, 575 (1985).
[5]Loren Pfeiffer, K. W. West, D. C. Joy, J. M. Gibson, and A. E. Gelman, Mater. Res. Soc. Symp. Proc. **53**, 29 (1986).
[6]M. W. Geis, C. K. Chen, H. I. Smith, P. M. Nitishin, B-Y. Tsaur, and R. W. Mountain, Mater. Res. Soc. Symp. Proc. **53**, 39 (1986). See also C. K. Chen, M. W. Geis, M. C. Finn, and B-Y. Tsaur, Appl. Phys. Lett. **48**, 1300 (1986).
[7]M. W. Geiss, H. I. Smith, and C. K. Chen, J. Appl. Phys. **60**, 1152 (1986).
[8]C. K. Chen, L. Pfeiffer, K. W. West, M. W. Geis, S. Darack, G. Achaibar, R. W. Mountain, and B-Y. Tsaur, Mater. Res. Soc. Symp. Proc. **53**, 53 (1986).
[9]D. C. Joy, D. E. Newbury, and D. L. Davidson, J. Appl. Phys. **53**, R81 (1982).
[10]A. E. Gelman, Loren Pfeiffer, G. H. Gilmer, K. A. Jackson, and K. W. West (unpublished).
[11]Loren Pfeiffer, A. E. Gelman, K. A. Jackson, and K. W. West, Mater. Res. Soc. Symp. Proc. **74**, 543 (1987).
[12]M. W. Geis, H. I. Smith, D. J. Silversmith, R. W. Mountain, and C. V. Thompson, J. Electrochem. Soc. **130**, 1178 (1983).
[13]Loren Pfeiffer, Scott Paine, G. H. Gilmer, Wim van Saarloos, and K. W. West, Phys. Rev. Lett. **54**, 1944 (1985).
[14]G. H. Gilmer, Mater. Res. Soc. Symp. Proc. **13**, 249 (1983).
[15]W. C. Dash, J. Appl. Phys. **30**, 459 (1959); B. Chalmers, *Principles of Solidification* (Wiley, New York, 1964), p. 307. See also K. T. Aust and B. Chalmers, Can. J. Phys. **36**, 977 (1958).